A&A 430, 691–700 (2005)
DOI: 10.1051/0004-6361:20041286

Astronomy & Astrophysics

Radiative properties of magnetic elements

II. Center to limb variation of the appearance of photospheric faculae

O. Steiner

Kiepenheuer-Institut für Sonnenphysik, Schöneckstrasse 6, 79104 Freiburg
e-mail: steiner@kis.uni-freiburg.de

Received 13 May 2004 / Accepted 15 September 2004

Abstract. For the understanding of more complex numerical simulation results, a basic facular model is created consisting of a magnetic flux sheet embedded in a plane parallel atmosphere. The atmosphere within the flux sheet is similar to the external one but shifted in the downward direction to result in a Wilson depression of 150 km. It is shown that the horizontal spatial extension of the contrast enhancement produced by this model increases from center to limb from a few tenths to up to 1″ as a consequence of enhanced radiation from the limbward surface outside (behind) the magnetic flux concentration. For a conceivable explanation of this radiative effect it is noted that a plasma parcel on the solar surface sideways of the flux sheet "sees" a more transparent sky in the direction towards the flux sheet compared to a direction away from it because of the rarefied atmosphere within the flux sheet. This facular model also produces a dark lane at the disk-center side (in front) of the flux sheet even though no flow is present. It it is due to the deep layers of the flux sheet that have a lower temperature gradient and are cooler than the surrounding atmosphere at equal geometrical depth. This implies that limb observations offer a glimpse of the "cool bottom" of magnetic elements. The center-to-limb variation of the size and the dark-lane effect derived from this basic model is recovered in a self-consistent, two-dimensional non-stationary simulation of a magnetic flux concentration. These findings are in excellent agreement with and provide an interpretation of recent observations of faculae at very high resolution by Lites et al. (2004, Sol. Phys., 221, 65).

Key words. Sun: magnetic fields – Sun: photosphere – Sun: faculae, plages

1. Introduction

Solar faculae appear as bright granules (facular granules) near the limb, when observed in white-light. They have attracted the interest of as early a solar observer as Johann Hieronymus Schroeter who published a monograph on solar faculae in 1789 (Schroeter 1789). Secchi (1872, Chap. 13) reports to see them at the disk center and to be able to see their appearance and disappearance at the solar limb. These early observations hint at the fact that faculae are a conspicuous feature of the visible solar disk, almost as conspicuous as sunspots. It is therefore not surprising that they play a key role in the solar radiance variation over a solar cycle and on shorter time scales (e.g. Fligge et al. 2000).

Much effort has been spent over the years to measure the continuum contrast of faculae as a function of limb distance. Results are diverse however, as the contrast is not only a function of the heliocentric angle, $\mu = \cos\theta$, but also of facular size, magnetic field strength, spatial resolution, etc. (Frazier 1971; Akimov et al. 1987; Moran et al. 1992; Ortiz et al. 2002). Also the measurements are prone to selection effects (Waldmeier 1949; Spruit 1976; Minasyants 1986; Auffret & Muller 1991; Centrone & Ermolli 2003; Vogler et al. 2004). Generally the contrast increases from close to neutral at the disk center, reaches a maximum around $\mu \approx 0.2 \ldots 0.4$, to fall off again towards the limb. Controversial measurements exist for the extreme limb, at which the contrast supposedly falls off but a further increase has been reported as well (Chapman 1970; Akimov et al. 1982; Chapman & Klabunde 1982; Akimov et al. 1987; Wang & Zirin 1987; Lawrence 1988; Chapman & Ziegler 1996; Sütterlin et al. 1999; Ahern & Chapman 2000; Centrone & Ermolli 2003). A monotonic increase up to the extreme limb is seemingly in support of the "hot-cloud" model, but can also be produced by the "hot-wall" effect as shown by Steiner & Stenflo (1990).

In this paper we concentrate on the appearance and size of faculae from center to limb rather than on the precise behaviour of the contrast and its dependency on field strength and size etc. While faculae at the disk center appear as facular points (Mehltretter 1974) with a size of a mere ≈0.2″ (Keil & Muller 1983), they are identified with "facular granules" at the limb, a term already used by Ten Bruggencate (1940). In the present context, the work by Auffret & Muller (1991) is noteworthy. They present center-to-limb variations (CLV) not only in contrast but also in size of network bright points (that are to be identified as network faculae close to the limb). They measure

an increase in size parallel and perpendicular to the solar limb, which they assert to be due to the preferential disappearance of small bright granules with decreasing limb distance but also to the contribution of a vertical dimension like that of a hot depression or of a hot cloud that impedes foreshortening effects to take place. The curious absence of foreshortening was also noticed by Adjabshirizadeh & Koutchmy (2002).

Recently, Lites et al. (2004) obtained images of faculae of unprecedentedly high spatial resolution with the newly commissioned 1-m Swedish solar telescope on La Palma (Scharmer et al. 2003). The faculae show at a heliocentric angle of $\mu = 0.54$ a size, measured perpendicular to the limb, of $\approx 0.5''$ or more. The facular brightening occurs at the disk center side of granules just limbward of the corresponding facular magnetic field. Also, the images reveal a thin dark lane at the disk center side of the facular brightening, separating it from the granule immediately centerward of it.

These observations are in apparent contradiction with the "hot wall" model (Spruit 1976) since the facular size far surpasses the vertical extension of the hot wall of ≈ 150 km. In Sect. 2 of this paper, however, it is shown that a basic facular model consisting of a magnetic flux concentration embedded in a plane parallel atmosphere (a "hot wall model") is capable of qualitatively reproducing both findings of Lites' high resolution observations. In Sect. 3 it is shown how the results of this abstract and inconsistent model carry over to self consistent but more complex and dynamic flux concentrations resulting from numerical simulations. Conclusions are given in Sect. 4.

2. Center to limb appearance of a static magnetic flux concentration

We first construct a basic, magnetohydrostatic model of a facula and then discuss its center to limb variation (CLV) of continuum contrast and total polarization. Although not self-consistent, this model provides us with a conceivable interpretation of a more complex and dynamic flux concentration resulting from fully self consistent numerical simulations presented in Sect. 3.

2.1. The model

Consider a plane parallel model atmosphere (Spruit's 1977 convection zone model (Spruit 1974), connected to the Harvard-Smithonian Reference Atmosphere, HSRA, of Gingerich et al. (1971)) in which embedded is a magnetic flux concentration in mechanical equilibrium. All variables of the computational domain depend only on two coordinates (in a Cartesian system), one horizontal, x, and one vertical, z (counted positive in the outward direction). The two-dimensional domain represents a slab that is cut perpendicular to the direction of y. Consequently, the model is suitable to represent a *magnetic flux sheet*, i.e., an elongated magnetic structure whose length is larger than its width. Ignoring any structure in the lane direction, it may represent small-scale magnetic flux that resides in the intergranular space and may fill it completely in active regions as can be expected of facular magnetic field that rises from integranular space like a curtain extending along several granules. It is less applicable to isolated flux tubes that are more commonly found at the vertices of intergranular lanes. But as we consider here exclusively radiative properties and not the dynamics of magnetic flux concentrations, this restriction is less of a concern.

The magnetic flux concentration is computed in the zeroth-order thin flux-sheet approximation. In this approximation the vertical component of the field strength, B_z, is constant as a function of x within the flux sheet, while it decreases with height, z, in accordance with

$$B_z^2(z) = 2\mu_0(p_\mathrm{e}(z) - p_\mathrm{i}(z)), \tag{1}$$

where $p_\mathrm{e}(z)$ and $p_\mathrm{i}(z)$ are the gas pressure as a function of height external to and within the magnetic flux sheet, respectively, and μ_0 is the magnetic permeability of vacuum. Equation (1) implies that $p_\mathrm{i} < p_\mathrm{e}\ \forall z$. $p_\mathrm{e}(z)$ is taken from our plane parallel model atmosphere, while the atmosphere within the magnetic flux concentration is similar to the external atmosphere but shifted in the downward direction by the "Wilson depression". More precisely, $p_\mathrm{i}(z)$ is computed from the internal temperature, $T_\mathrm{i}(z)$, using the equation of state for the solar plasma derived from the ideal gas law and Saha's equation and given the gas pressure at a reference level. In the optically opaque layers below $\tau_c = 1$, the internal temperature as a function of height, $T_\mathrm{i}(z)$, is, up to a translation in z, identical to that of the external atmosphere, $T_\mathrm{e}(z)$, while above this level we assume temperature equilibrium, $T_\mathrm{i}(z) = T_\mathrm{e}(z)$. These two regimes are connected by a tanh-transition. Formally, $T_\mathrm{i}(z)$ is given by

$$T_\mathrm{i}(z) = \begin{cases} T_\mathrm{e}(z+W) & \text{for} \quad z \le z_0 - D/2 \\ T_2 + (T_1 - T_2)\dfrac{1}{2}\left(1 + \tanh\left[\dfrac{4}{D}(z - z_0)\right]\right) & \\ T_\mathrm{e}(z) & \text{for} \quad z \ge z_0 + D/2, \end{cases} \tag{2}$$

where T_1 and T_2 are chosen such that the transition matches exactly the value of T_i at $z_0 - D/2$ and $z_0 + D/2$ given by the connecting formulas. In the following, the reference height for the transition, z_0, is always set at the height where $\tau_c = 1$ in the external atmosphere and $D = 2W$, where $W = 150$ km, which leads to a field strength at $z = z_0$ of approximately 0.16 T. The internal gas pressure at the reference level z_bot is given by $p_\mathrm{i}(z_\mathrm{bot}) = p_\mathrm{e}(z_\mathrm{bot} + W)$. W approximately corresponds to the "Wilson depression", i.e., the depth by which the surface of optical depth unity is depressed at the location of the magnetic flux concentration. It would be identical to the "Wilson depression" if we had $T_\mathrm{i}(z) = T_\mathrm{e}(z + W)\ \forall z$. This construction implies that the gas pressure and density within the flux sheet is always smaller than the corresponding values in the external atmosphere at equal geometrical height.

The full computational domain has a size of 2400 km in the horizontal and 1400 km in the vertical direction, of which 600 km are above and 800 km below the optical depth $\tau_c = 1$ of the external atmosphere. However, only a limited height range around the level of optical depth unity really determines the radiative property of the flux sheet. Density and temperature jump at the flux-sheet boundary are smoothed according to Eq. (3) of Knölker et al. (1988), where $\delta = 0.3$, meaning that

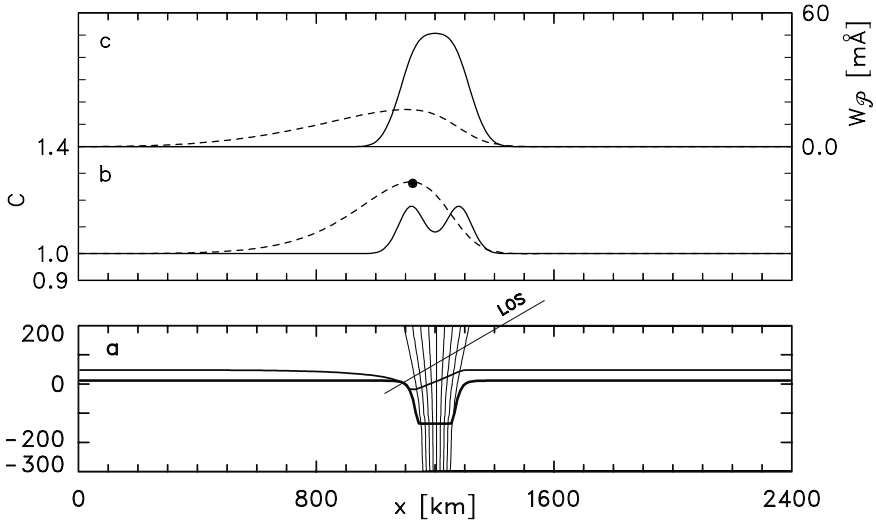

Fig. 1. a) Section of the full computational domain with the magnetic flux sheet in the center, indicated by magnetic lines of force. The surface of optical depth $\tau_c = 1$ for vertical lines of sight (disk center) is indicated by the thick curve. The thin curve gives the same optical depth level for lines of sight running from the top right to the bottom left under an angle of $\theta = 60°$ to the vertical. **b)** Continuum contrast, defined according to Eq. (3), for vertical lines of sight ($\mu = 1$, solid curve) and for inclined lines of sight with $\mu = 0.5$ (dashed curve). All values of the dashed curve left of the black dot belong to lines of sights left of the one indicated in panel a). **c)** Equivalent width of the total polarization of Fe I 630.25 nm, according to Eq. (4), for the cases of $\mu = 1$ (solid curve) and $\mu = 0.5$ (dashed curve).

this boundary layer has a width of about one third of the flux-sheet's half width. No such transition was applied to the magnetic field. This transition layer destroys mechanical equilibrium but it is probably more realistic than a sharp discontinuity (Schüssler 1986; Hirayama 1992) and it guarantees smooth integration of the radiative transfer equation along lines of sight that cross the flux-sheet boundary.

2.2. Center to limb variations

Figure 1a shows a section of the full computational domain with the magnetic flux sheet in the center, indicated by magnetic lines of force. It has a width of ≈170 km at the level where $\tau_c = 1$ in the external atmosphere. The surface of $\tau_c = 1$ for vertical lines of sight (disk center) is indicated by the thick curve. It shows a "Wilson depression" of 141 km. The thin curve gives the same optical depth level for lines of sight running from the top right to the bottom left under an angle of $\theta = 60°$ to the vertical. This corresponds to an observation off disk center at the heliocentric angle $\mu = 0.5$, where the disk center lies to the right and the limb to left hand side. Here and in the following we use Rosseland's mean opacity for computing τ_c.

Figure 1b shows the continuum contrast at $\lambda = 630.25$ nm for the two disk positions $\mu = 1$ (solid curve) and $\mu = 0.5$ (dashed curve). The contrast is here defined as a simple intensity ratio,

$$C(x) = I_c(x)/I_{c0}, \tag{3}$$

where I_c is the outwardly directed intensity along the line of sight at position x computed with the help of the Rosseland mean opacity and I_{c0} is the corresponding intensity emerging from the plane parallel, unperturbed, external atmosphere. The contrast has been convoluted with a Gaussian of half width $36/\mu$ km in order to mimic a finite spatial resolution of ≈0.1″. For better comparison, the dashed curve has been shifted in the x-direction to match the contrast rise at the disk-center side.

The contrast at the disk center shows the typical double humped profile already shown by Caccin & Severino (1979), Chapman & Gingell (1984), or Deinzer et al. (1984). The two humps originate from the "hot walls" of the flux-sheet depression. At full spatial resolution the central dip returns almost back to $C = 1$ but does not do so exactly since the temperature of the internal atmosphere drops less steep than $T_e(z)$ in the height range from $z = -150$ km to $z = 150$ km in order to achieve temperature equilibrium for $z \geq 150$ km. In reality the central contrast can be expected to be <1 because of the reduced energy transport within the flux sheet in the deep convective layers, where the present approach with the shifted atmosphere might well overestimate the temperature. In fact this approach implicitly assumes that the energy transport in the vertical direction within the flux sheet is not throttled by the magnetic field at all.

The contrast at $\mu = 0.5$ is enhanced over a wider distance than at the disk center and the maximum value is higher. The latter finding is in accordance with the well known observational fact that the contrast of facular points increases from disk center out to $\mu \approx 0.3$–0.4. The larger width of the contrast enhancement for $\mu = 0.5$ is in accordance with the recent observation of Lites et al. (2004) that show facular sizes (perpendicular to the limb) of 0.5″ and more at $\mu = 0.54$.

The contrast profile at $\mu = 0.5$ is asymmetric with a steep increase at the disk center side and a gentle decrease on the limb side. The wide extension of the contrast enhancement towards the limb can also be seen from the corresponding $\tau_c = 1$ surface that starts to drop into deeper (hotter) layers already ≈700 km limbward of the flux-sheet center. At the disk-center side it is back to the value of the plane-parallel external atmosphere closely outside the magnetic flux sheet. This shape of the contrast profile is also a characteristic of the two-component models of Caccin & Severino (1979) and Chapman & Gingell (1984) and of the two cross-sections shown by Lites et al. (2004).

The reason for this behaviour of the τ_c-surface is that a line of sight that traverses the photospheric layers of the flux sheet encounters there a reduced density, which reduces the opacity. If it traverses below $z = 150$ km it additionally encounters lower temperatures, which further decreases the opacity. Hence, the optical path of the section through the flux sheet is smaller than it is of a corresponding distance in the

external atmosphere so that the optical scale becomes a little bit stretched into deeper, thus hotter layers in the atmosphere limbward of the flux sheet. From a location at the solar surface and sideways of the flux sheet a plasma parcel "sees" a more transparent sky in the direction across the flux sheet compared to a direction under equal zenith angle but away from it. Correspondingly, from a wide area surrounding the magnetic flux sheet or flux tube, radiation escapes more easily in the direction of the flux sheet/tube. Thus, the cross-sectional area of a single flux sheet/tube for influencing the radiative escape is not confined to the magnetic field concentration but encompasses a much wider area surrounding it. In the present case with a flux-sheet width of approximately 170 km at $\tau_e = 1$ this area is for rays with $\theta = 60°$ approximately 2×700 km wide, i.e., eight times as large.

For the heliocentric angle $\mu = 0.5$, the line of sight labeled LOS in Fig. 1a, demarcates the region to the right of it, where the "hot wall" of the flux-sheet interface causes enhanced radiation escape, from the region to the left of it, where radiation preferentially escapes along lines of sight that traverse the magnetic sheet of reduced opacity. The demarcating line of sight gives rise to the maximal contrast value marked with a black dot in Fig. 1b. This demonstrates that the steep rising part of the contrast curve at the disk-center side is caused by the "hot wall" of the flux-sheet interface, the wider, gently fading brightening on the limbward side originates from a region outside the flux sheet proper and is due to the optical transparency of the magnetic flux sheet. It is not caused by a "hot cloud" in the pathway of any line of sight, since $T_i(z) \leq T_e(z)\ \forall z$ in the present model.

The influence that the magnetic flux sheet has on the radiation from the solar surface causes the cooling rate to depend on distance from the flux sheet axis and hence, a horizontal gas-pressure gradient builds up that will drive a flow of plasma directed towards the flux sheet. At this point the hydrostatic model set-up of Sect. 2.1 must break down: in fact it is even out of radiative equilibrium because of the radiative perturbation caused by the magnetic flux sheet. In Sect. 3 we will analyze a model that does not suffer this deficit. The results derived in this section, however, will be useful for the understanding of this more complex model and it turns out that they capture the essential physics of the appearance of faculae.

Subject to this limitation, the model therefore suggests that what is seen of faculae near the limb is not only a "hot wall" but a bright granule limbward to the magnetic flux concentration, which presence causes the granule to become bright. That one sees regular photospheric but brighter than normal granulation across some atmospheric perturbation was already conjectured by Chevalier (1912), Unsöld (1938), and Yudina (1976). However, Spruit (1976), Caccin & Severino (1979), and Chapman & Gingell (1984) first stressed the optical implications of a partially evacuated magnetic flux concentration. Such a perturbation in a two- or three-dimensional atmosphere causes a channeling of the radiative energy flux as is shown in Cannon (1985), Kneer & Trujillo-Bueno (1987), or Hasan et al. (1999) in the context of magnetic flux tubes. The center to limb increase in width of the contrast enhancement of a flux tube/sheet can also be seen from Fig. 17 of Deinzer et al. (1984)

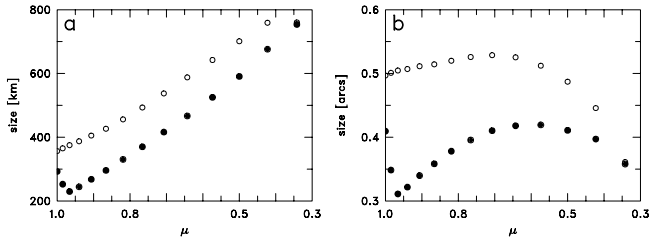

Fig. 2. Width of contrast enhancement (solid dots) and of total polarization (circles) from center to limb for the model shown in Fig. 1. Size measured **a)** parallel to the solar surface; and **b)** in the plane of the sky.

and from Figs. 9 and 10 of Bruls & von der Lühe (2001), although these authors did not explicitly discuss its implication for the appearance of solar faculae.

Figure 1c shows the equivalent width of the total polarization

$$W_{\mathcal{P}} = \int \sqrt{V^2 + Q^2 + U^2}\, \mathrm{d}\lambda, \tag{4}$$

where V, Q, and U are the Stokes parameters for circular and linear polarization normalized to the nearby continuum and the integral is taken over the full profile width of the line Fe I 630.25 nm. Both curves approximately follow their respective counterparts in continuum contrast but the polarization signal strongly decreases from the disk center to $\mu = 0.5$ and the limbward decrease is slightly less steep than the corresponding decrease in continuum contrast. No significant spatial shift of the polarization signal with respect to the continuum signature can be predicted when going from center to limb but the polarization signal can be expected to show a slightly more extended limbward tail compared to the continuum brightening.

Despite the confined nature of the magnetic flux concentration whose magnetic field strength assumes essentially a box profile at the solar surface, the polarization signal shows a smooth distribution even at disk center. This is because the flux sheet expands with height and lines of sight in the periphery of it sample weak field in higher layers so that the polarization signal smoothly decreases with increasing distance from the flux-sheet axis. Thus, caution is indicated when inferring magnetic structuring from polarization signals: a smooth distribution of magnetogram signals does not proof the absence of structuring.

Figure 2 shows the width of the contrast enhancement (solid dots) and of the total polarization (circles) from center to limb as a function of μ for the same model as shown in Fig. 1. The width of the contrast enhancement is defined by the distance over which the contrast surpasses a value of $C_{\mathrm{lim}} = 1.05$. Similarly, the width of the polarization signal is given by the limiting value $W_{\mathcal{P}\,\mathrm{lim}} = 0.5$ pm (5 mÅ). Data prepared to mimic $0.1''$ resolution have been used. Figure 2a shows the width as measured parallel to the solar surface, giving a measure for the size of the cross-sectional area impacted by the presence of the magnetic flux sheet. Figure 2b shows the apparent width of this area in the plane of the sky, which corresponds to the widths of Fig. 2a, multiplied by μ. The drop in width of the contrast enhancement from disk center to $\mu \approx 0.96$ ($\theta = 15°$),

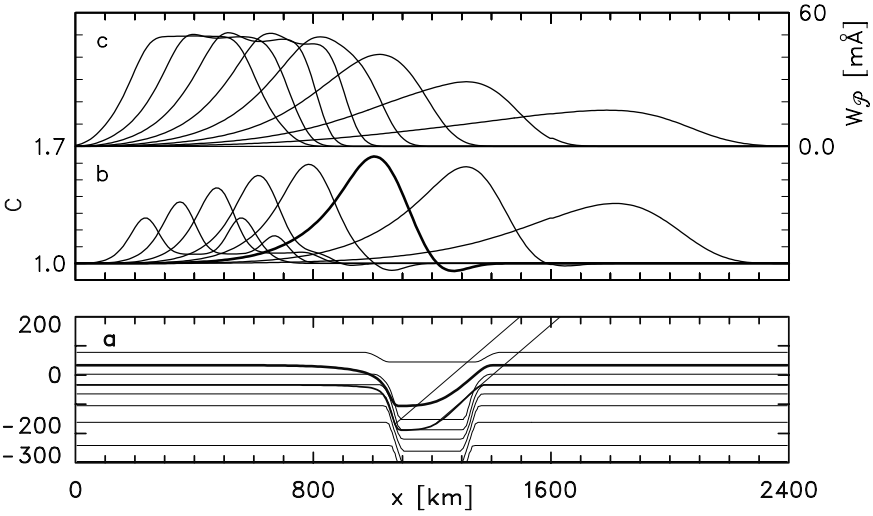

Fig. 3. a) Section of the full computational domain with a magnetic flux sheet in the center. Indicated are isothermal contours and two surfaces of optical depth $\tau_c = 1$ and $\tau_c = 5$, both computed for lines of sight running from the top right to the bottom left under a zenith angle of $\theta = 50°$. **b)** Continuum contrast, defined according to Eq. (3), for lines of sight with $\theta = 0° \ldots 70°$ in steps of 10°. For the prominent profile belonging to $\theta = 50°$, the region where $C < 1$ is bounded by the two lines of sight indicated in panel a). **c)** Equivalent width of the total polarization, according to Eq. (4), for the same azimuth angles as in panel b).

is caused by gradual foreshortening and final disappearance of the disk-center side "hot wall". Further out, this disappearance from sight is compensated for by an ever better view of the limbward "hot wall" and an increase in size of the brightening of the limbward area behind the flux sheet. Different from the contrast signal, the width of the total polarization monotonically increases from center to limb and it is always larger than the with of the contrast enhancement. The variation of both widths is less dramatic when measured as apparent width in the plane of sky. This measure increases from 220 km (0.3″) to 300 km (0.4″) at $\theta = 55°$ and decreases further out towards the limb. With a Wilson depression of 150 km and a flux-sheet width of 170 km, the apparent size of the depression wall starts to decrease rapidly below $\mu = 0.66$ because of obscuration by the centerward "edge" of the depression and a mere 55 km of it remains visible at $\mu = 0.3$. Thus, beyond $\mu = 0.66$ the apparent size of faculae remains almost constant because of the brightening of the area limbward of the flux sheet proper.

The fit by Auffret & Muller (1991) of the apparent size of faculae perpendicular to the limb increases from 0.4″ to 0.53″ from the disk center to $\mu = 0.4$, slightly decreasing out to $\mu = 0.17$. Considering the large scatter in these measurements and the fact that we consider here one single flux sheet instead of an ensemble of flux sheets of diverse parameters, the present model is in good agreement with these findings.

2.3. The facular lane

Figure 3a shows isotherms together with two optical depth surfaces of $\tau_c = 1$ and $\tau_c = 5$ computed for lines of sight running from top right to bottom left under a zenith angle of $\theta = 50°$. Different from the model discussed in the previous section, the flux sheet has a larger width of ≈300 km at the level of $\tau_e = 1$, all other properties being identical. The contrast profiles for $\theta = 0° \ldots 70°$ in steps of 10° are shown in Fig. 3b, where the profile belonging to $\theta = 50°$ is emphasized. Again, the profiles are Gaussian convoluted for a spatial resolution of 0.1″ and are all shifted to the left by an equal amount to fit into the same panel. One can see again the characteristic limbward tail of the contrast profile and the corresponding plunge of the iso-τ surface into hotter layers. On the disk-center side, however, profiles with $30° \lesssim \theta \lesssim 60°$ show within a narrow region a contrast of $C < 1$, giving rise to a "dark lane" centerward (in front of) the facular brightening.

The region within which the dark lane is formed is indicated in Fig. 3a for the case of $\theta = 50°$, where the two lines of sight mark the edges of the dark region where $C = 1.0$ at full spatial resolution. Lines of sight within this region traverse layers of the flux sheet where the temperature gradient is smaller than at corresponding optical depths in the external atmosphere as can be seen from the isotherms. Their optically deep part comes to lie into the cool deep layers of the flux-sheet interior, while their upper, optically more transparent part travels through the plane parallel normal external atmosphere. On the other hand, these lines of sight do not yet "see" the "'hot wall" of the flux-sheet interface that is still hidden from sight in large optical depths. Hence, one can say that they sample the cool deep layers of the magnetic flux sheet.

As mentioned in Sect. 2.2 the energy flux in the deep layers of the flux sheet is probably overestimated by the present model so that the "bottom" of the depression should in reality be cooler than it is. If so, the contrast deficit in the dark lane is further pronounced, i.e., the lane darker. A low temperature gradient in the deep layers of faculae was derived from contrast measurements of two widely separated continuum passbands (Foukal & Duvall 1985; Nishikawa & Hirayama 1990) but is also an invariable outcome of Stokes inversion techniques applied to magnetic elements (Solanki 1986; Keller et al. 1990; Bellot Rubio et al. 2000). Infrared measurements of facular regions at or close to the opacity minimum at 1.63 μm of Foukal et al. (1989, 1990); Moran et al. (1992) and Wang et al. (1998) have given low contrast at the disk center, indicating that in these layers faculae are cooler than the surroundings even at equal optical depth.

Figure 3c shows the equivalent width of the total polarization corresponding to the profiles of Fig. 3b. No obvious signature of the dark lane is visible.

A dark lane disk centerward of the facular brightening was recently shown to exist by Lites et al. (2004), having a width approaching the spatial resolution of the telescope of 0.12″

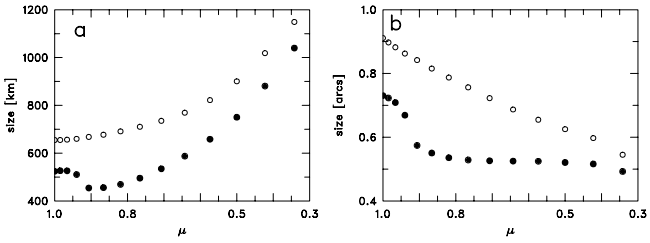

Fig. 4. Width of contrast enhancement (solid dots) and of total polarization (circles) from center to limb for the model shown in Fig. 3. Size measured **a)** parallel to the solar surface; and **b)** in the plane of the sky.

and a contrast deficit of approximately 0.04. The corresponding values from the present model with a spatial resolution of 0.009″ at heliocentric distance $\mu = 0.5$ are 0.09″ and 0.1, changing to 0.14″ and 0.045 at 0.1″ resolution. A dark lane is also an integral feature of the facular models of Caccin & Severino (1979) and Chapman & Gingell (1984) but they did not further investigate the origin of this phenomenon, although the phenomenon was at that time already observed by R. Muller (Spruit 1977).

Figure 4 shows the width of the contrast enhancement and that of the polarization from center to limb for the model of Fig. 3, where the same definition is used as for Fig. 2. Again, the apparent size of the contrast enhancement remains almost constant from $\mu = 0.9$ outward. At the disk center the contrast shows the characteristic double humped profile (see Fig. 3) where the two humps are separated by more than 300 km, which explains the large size for $\mu = 1$ in Fig. 4. This size persists to almost $\theta = 20°$ ($\mu = 0.95$), a consequence of the stronger expansion of the flux sheet with height compared to the thinner model of Fig. 1. Likewise, the width of the total polarization signal always surpasses that of the contrast enhancement. Its apparent size monotonically decreases from 650 km at the disk center to 400 km at $\mu = 034$.

3. Center to limb appearance of a dynamic magnetic flux concentration

In the following we repeat the analysis of Sect. 2 but this time applied to stills of a numerical radiation-hydrodynamic simulation of a magnetic flux sheet embedded in and in interaction with nonstationary convection. The aim is to test if the results found in the preceding section carry over to this self-consistent model. Results will be discussed in the light of the insights gained in Sect. 2.

3.1. The model

We consider the eight snapshots a)–h) of Fig. 1 of Steiner et al. (1998). The details of this simulation are described in this paper, so that we give here just a brief summary.

Starting from a partially evacuated magnetic flux sheet embedded in and in mechanical equilibrium with a plane parallel standard solar atmosphere (similar to the model of Sect. 2), the non-stationary evolution of this configuration is followed by numerical integration of the system of the magnetohydrodynamic equations. The non-stationary evolution comes about because of the motion that develops in the convectively unstable layers below $\tau_c = 1$. The energy equation is solved including hydrogen ionization and radiative transfer in the grey approximation to account for interaction of radiation with matter. The computational domain is of the same dimension as that of Sect. 2.1. After an initial transient phase, a dynamical interaction of the magnetic element with granular convection evolves, which can be characterized by the following phenomena: (1) a swaying motion of the flux sheet due to the asymmetrical convective flow; (2) shocks inside and outside the flux sheet; and (3) downflow jets at the interface between the flux sheet and its environment. The phenomena can be followed in detail in the video tape accompanying issue 495 of The Astrophysical Journal. The "Wilson depression" measured as the maximal $\tau = 1$-depression relative to the actual horizontal mean height of the $\tau = 1$-surface (including the depression) varies over the simulation run from 153 to 319 km with a mean of 217 km. The $\tau = 1$-surface varies within a hight range of 444 km. These numbers are in good agreement with corresponding results from 3-D simulations (Carlsson et al. 2004).

3.2. Center to limb variations

Figure 5 shows 8 stills of the simulation that are separated in time by approximately 2 min. Each set of panels a)–h) of Fig. 5 consists of the bottom panel showing magnetic lines of force of the flux sheet together with two surfaces of optical depth unity, the middle panel showing the continuum contrast at 630.25 nm, and the top panel the equivalent width of the total polarization for the line Fe I 630.25 nm, each time for the same two viewing angles. The solid curves correspond to vertical lines of sight (disk center, $\mu = 1.0$), the dashed curves to lines of sight inclined by $\theta = -60°$ ($\mu = 0.5$) having a direction from top left to bottom right. Contrast and polarization profiles are convoluted by a Gaussian mimicking a spatial resolution of 0.1″.

In each snapshot a)–h) the disk-center contrast-profile reflects the presence of the magnetic flux sheet by a more or less prominent enhancement, at least with respect to the close surroundings. These surroundings, on the other hand, are always dark because of the persistent cool downdraft jets that form at the interface to the flux sheet. They have typically a width around 100 km. The double humped nature of the contrast profile is not visible here while only signs of it can be seen at the maximal spatial resolution of the model of 10 km. In all cases, with the exception of panel set e), the contrast enhancement is higher and wider at $\mu = 0.5$, i.e., for observations near the limb, compared to disk-center observations. Panel e) is exceptional because of the strong bending of the flux sheet that exposes an extended area of "hot wall" at a favourable angle towards the observer looking vertically downward, similar to an observation off disk center in the normal case.

The distance over which the presence of the magnetic flux sheet causes $C > 1$ is highlighted in bold for the case of $\mu = 0.5$. With the exception of case e), each of the dashed contrast profiles shows the typical shape discussed in Sect. 2.2: a steep

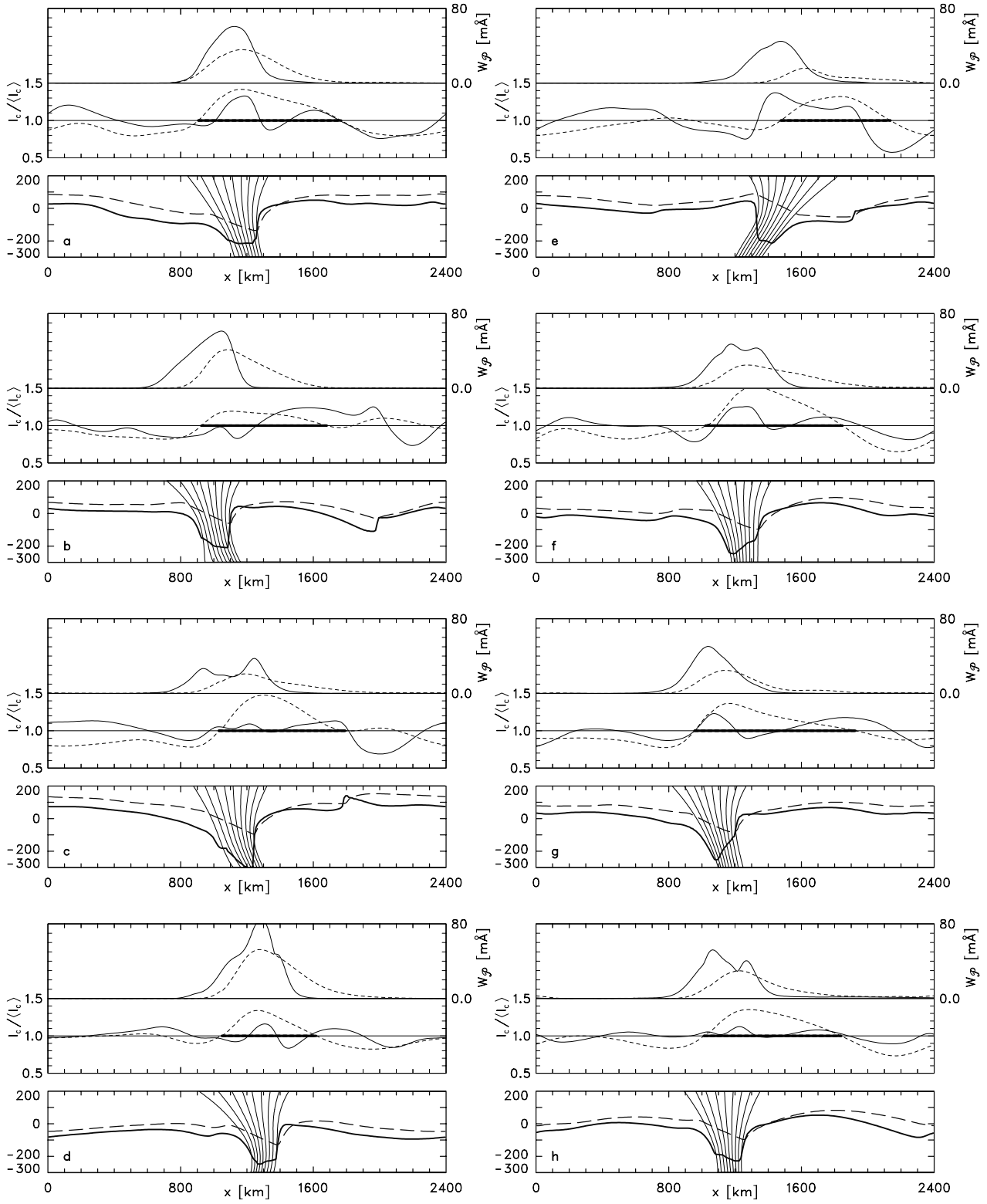

Fig. 5. The set of panels **a)**–**h)**, each referring to stills of a numerical simulation separated in time by approximately 2 min. Of each set the bottom panel shows magnetic lines of force of the flux sheet together with two surfaces of optical depth unity, the middle panel shows the continuum contrast, and the top panel the equivalent width of the total polarization for the line Fe I 630.25 nm, each for the same two viewing angles. The solid curve corresponds to vertical lines of sight (disk center, $\mu = 1.0$), and the dashed curve to lines of sight inclined by $\theta = -60°$ ($\mu = 0.5$) having a direction from top left to bottom right. Contrast and polarization profiles are convoluted by a Gaussian mimicking a spatial resolution of 0.1″. The heavy horizontal lines indicate the width of the contrast enhancement for the case of $\mu = 0.5$. The bottom panel shows just part of the full computational domain of 2400 × 1400 km.

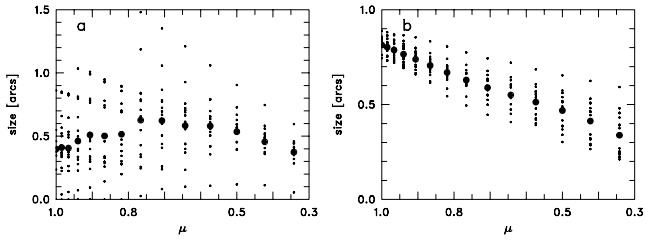

Fig. 6. Apparent size of contrast enhancement **a**) and polarization signal ($\mathcal{P}$(Fe I 630.25)) **b**) as a function of disk position μ. For each $\mu < 1$ there are 16 points from the 8 snapshots a)–h) of Fig. 5 and two opposite directions. The heavy dots show arithmetic means.

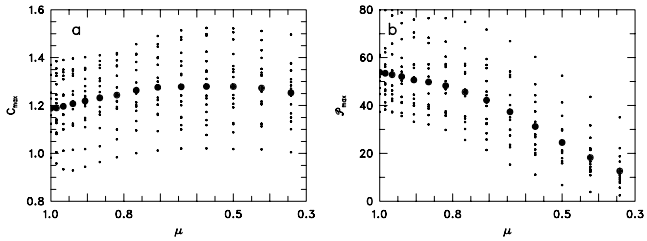

Fig. 7. Maximum contrast value **a**) and maximum polarization signal ($\mathcal{P}$(Fe I 630.25)) **b**) as a function of disk position μ.

rise on the disk-center side (left hand side in Fig. 5) and a gentle fading on the limbward side. Considering that the magnetic flux sheet is always framed by two granules, this means that the granule limbward of the flux sheet appears brighter than a regular granule with a gentle decline in brightness over about half of its size, exactly what is observed by Lites et al. (2004). This property of the appearance of faculae was well expressed by the term "facular granule" in the past (Chevalier 1912; Ten Bruggencate 1940; Bray & Loughhead 1967) as it is to a large extent a photospheric granule that appears bright limbward and across a magnetic flux concentration, giving rise to the facular phenomenon. Note in the bottom panel that the extended tail of the limbward brightening is reflected by the decreasing distance of the two iso-τ surfaces towards the flux sheet. They finally cross over near the "hot-wall" of the flux-sheet interface.

The polarization signal for the case of $\mu = 0.5$ follows approximately the run of the contrast profile as was already found for the model of Sect. 2. However, it cannot be said that its limbward decline is less steep than that of the contrast profile. Again, we note the relatively smooth distribution of total polarization despite the discrete nature of the flux sheet.

Figure 6 shows the apparent size from center to limb of the contrast enhancement and the total polarization signal. Plotted are all the data for lines of sight under zenith angles $\theta = 0^\circ, \pm 10^\circ \ldots \pm 70^\circ$, separated by 10° for all snapshots a)–h) of Fig. 5. For each discrete μ-value the arithmetic mean is indicated by a heavy dot. As for Figs. 2b and 4b the apparent mean size of the contrast enhancement stays relatively constant out to $\mu = 0.3$. The mean extension of the facular brightening as measured parallel to the surface (not shown here) monotonically increases to 800 km at $\mu = 0.3$. As in Fig. 4b the width of the polarization signal monotonically decreases.

Figure 7 shows the center to limb values of the maximum contrast (a) and equivalent width of total polarization for Fe I 630.25 nm (b). While the mean peak contrast of 1.28 might be still in line with the corresponding value of Lites et al. (2004) of 1.15, the maximum contrast occurs at about $\mu = 0.65$, which is too close to the disk center compared with observations. According to Spruit (1976), the position of the maximum contrast is essentially determined by the ratio of tube diameter to Wilson depression (the critical angle for which the bottom becomes just obscured), which hints at the present flux sheet being too small.

Plotting the maximum contrast times the width of the contrast enhancement for a measure of the visibility of a facula against μ predicts the maximum visibility of faculae to occur closer to the disk center compared to the location of maximum contrast, because of the size compensating for the lack of contrast. A distinction between visibility and contrast was made by Waldmeier (1949) who finds maximal visibility closer to the disk center too.

3.3. The facular lane

Figure 8 shows surfaces of optical depth $\tau_c = 1$, contrast profiles for the continuum at 630.25 nm, and equivalent widths of total polarization of Fe I 630.25 nm for the case of panel h) of Fig. 5 and for two viewing angles. The solid curves refer to $\theta = +45^\circ$ and dashed curves to $\theta = -45^\circ$, corresponding to viewing from top right to bottom left and from top left to bottom right, respectively. Also shown in the bottom panel are magnetic lines of force of the flux sheet and the velocity field of the plasma flow. Both contrast profiles show the brightening of the disk-center side of the granule limbward to the flux sheet and the dark facular lane in front of it. The two lines of sight that limit the dark lane region where $C < 1$ are drawn in the bottom panel together with the line of sight of least intensity in between them. From this plot we see that the dark lane phenomenon is not exclusively caused by the cool deep layers of the flux sheet interior (as was found in Sect. 2.3) but to a large degree the area in the close vicinity of the flux sheet contributes to it. The minimum intensity arises from these surroundings rather than from the flux-sheet interior. There, the radiation is strongly anisotropic with preferential photon escape towards the flux sheet and a partially compensating deficit away from it (along centerward directed lines of sight), causing the extra width of the dark lane. According to Spruit (1977) most of the extra energy loss is efficiently replenished by the convective heat transport taping from the large heat reservoir of the convection zone so that a net heat leak exists and only a small part is compensated by the dark lane or ring of lower surface temperature in the surroundings of the flux concentration. This is the reason why the basic model of Sect. 2, where this compensating effect is neglected, still fares so well and yet it also shows a dark lane, alone by virtue of the atmosphere in the flux-sheet interior.

Different from the static model of Sect. 2, the radiative escape from the "hot walls" and its limbward extension must be replenished by lateral convective energy transport. As this

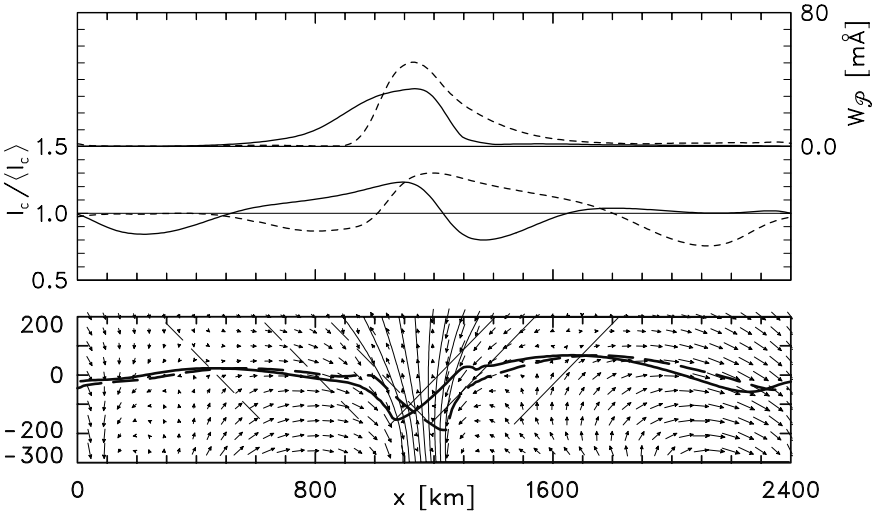

Fig. 8. Surfaces of optical depth $\tau_c = 1$ (*bottom*), contrast profiles (*middle*), and equivalent widths of total polarization of Fe I 630.25 nm (*top*) for the case of panel **h)** of Fig. 5 and for two viewing angles. The solid curves refer to $\theta = +45°$ and dashed curves to $\theta = -45°$ corresponding to viewing from top right to bottom left and from top left to bottom right, respectively. Also shown in the bottom panel are magnetic lines of force of the flux sheet, the velocity field of the plasma flow, and the two lines of sight that limit the facular lane region where $C < 1$ together with the line of sight of least intensity, for both viewing angles.

material cools off at the flux sheet interface it becomes dark and heavy giving rise to the downflow jets. This does not mean that the "hot walls" become dark as one still sees subsurface layers at the walls of the Wilson depression but these layers are less hot than they are in the unperturbed layers far away from the flux sheet.

4. Conclusions

From a basic facular model consisting of a magnetostatic flux sheet embedded in a plane parallel atmosphere and from a more complex but fully self-consistent, numerical simulation of a non-stationary flux concentration in dynamic interaction with convective motion the following results are obtained by radiation-transfer analysis along lines of sight of various inclinations for a simulation of the center to limb behaviour:

Off disk center, the contrast shows a steep increase at the disk-center side and a gentle fading over a wide distance on the limbward side. The steep increase in brightness comes from the "hot wall" of the flux-sheet interface, the wide brightening limbward of it, however, originates from a region outside the flux sheet proper and is due to the reduced opacity that photons experience when traveling along lines of sight that traverse the flux sheet in photospheric layers. For a more conceivable explanation one can say that from a location at the solar surface and sideways of the flux sheet the sky is more transparent in the direction across the flux sheet compared to an equal altitude direction away from it, leading to enhanced radiation escape in this direction. Thus, a single flux sheet/tube influences the radiative escape in a cross-sectional area that is much wider than the magnetic field concentration proper. As the limbward brightening extends over a spatial distance of roughly 0.5−1″ it encompasses about half a granule, the disk center side of the granule just limbward of the corresponding facular magnetic field. It could be called a facular granule. Reported time scales of facular granules of about 20 min (Muller 1977; Hirayama 1978) must correspondingly pertain to the associated magnetic field rather than to the granule itself, although a persistent granular flow impinging on the flux sheet boundaries is driven by the cooling at the "hot walls" (Steiner et al. 1998).

Going from center to limb, the increasing obscuration of the "hot wall" by the disk-center "edge" of the flux-sheet depression is compensated for by the increasing width of the limbward brightening. Therefore, the apparent (measured in the plane of the sky) size of faculae perpendicular to the solar limb stays fairly constant over a wide distance towards the limb as observed (Auffret & Muller 1991) and different from what would be expected of "hot wall" obscuration or foreshortening effects.

Very close to the disk center the spatial extent of the contrast enhancement decreases with increasing heliocentric angle because of gradual disappearance (foreshortening) of the disk-center side "hot wall". This effect, however, is less present in the dynamic models, where the flux sheet at different time instances has various inclination angles with respect to the vertical. The width of the polarization signal generally surpasses that of the continuum signal and monotonically drops from center to limb.

On the disk-center side of the magnetic flux sheet the intensity drops below average, leading to a narrow dark facular lane, that was recently shown to exist by Lites et al. (2004). It arises from the low temperature gradient of the flux-sheet atmosphere in the height range of optical depth unity. In a narrow region, photons from this height range can escape along lines of sight that travel through this "cool bottom" of the flux sheet. The static models produce facular lanes of width below 0.1″ with an intensity deficit of about 4%, while the dynamic models show an intensity deficit up to ≈20% and width of up to 0.35″. The increase in lane width in the dynamic models is due to the persistent downflows that exist at the flux sheet interface, which appears at the disk center much like an intergranular lane.

Two very recent letters, Keller et al. (2004) and Carlsson et al. (2004), treat the appearance of photospheric faculae too. The papers show synthetic continuum, and *G*-band contrasts, respectively, from 3-D magneto-convective simulations. Keller et al. (2004) come to very similar conclusions with respect to the origin of the facular brightness and the dark lane as comes the present paper but there exist differences too, notably the contrast-profile shape that does not show the characteristic asymmetric shape found in the present work and the

distinctly higher peak contrast. The effect of a magnetic flux concentration on the radiation from its surrounding area can also be studied from Fig. 3 of Carlsson et al. (2004) which shows the G-band formation height for $\mu = 1.0$ and 0.6 with a similar behaviour of their relative distance as for the continuum in Fig. 1 of the present paper.

Acknowledgements. I thank B. W. Lites for providing me early results of his observations, thus initiating this work, and J. Bruls for detailed comments on a draft of this paper.

References

Adjabshirizadeh, A., & Koutchmy, S. 2002, in ESA SP-506, Solar Variability: From Core to Outer Frontiers, 415
Ahern, S., & Chapman, G. A. 2000, Sol. Phys., 191, 71
Akimov, L. A., Belkina, I. L., & Dyatel, N. P. 1982, Soviet Astron., 26, 334
Akimov, L. A., Belkina, I. L., Dyatel, N. P., & Marchenko, G. P. 1987, Soviet Astron., 31, 64
Auffret, H., & Muller, R. 1991, A&A, 246, 264
Bellot Rubio, L. R., Ruiz Cobo, B., & Collados, M. 2000, ApJ, 535, 475
Bray, R. J., & Loughhead, R. E. 1967, The solar granulation, The International Astrophysics Series (London: Chapman & Hall)
Bruls, J. H. M. J., & von der Lühe, O. 2001, A&A, 366, 281
Caccin, B., & Severino, G. 1979, ApJ, 232, 297
Cannon, C. J. 1985, The transfer of spectral line radiation (Cambridge: University Press)
Carlsson, M., Stein, R. F., Nordlund, Å., & Scharmer, G. B. 2004, ApJ, 610, L137
Centrone, M., & Ermolli, I. 2003, Mem. Soc. Astron. It., 74, 671
Chapman, G. A. 1970, Sol. Phys., 14, 315
Chapman, G. A., & Gingell, T. W. 1984, Sol. Phys., 91, 243
Chapman, G. A., & Klabunde, D. P. 1982, ApJ, 261, 387
Chapman, G. A., & Ziegler, B. 1996, Sol. Phys., 168, 259
Chevalier, S. 1912, Ann. de l'Obs. de Zô-sè, 8, C1
Deinzer, W., Hensler, G., Schüssler, M., & Weisshaar, E. 1984, A&A, 139, 435
Fligge, M., Solanki, S. K., & Unruh, Y. C. 2000, A&A, 353, 380
Foukal, P., & Duvall, T. 1985, ApJ, 296, 739
Foukal, P., Little, R., Graves, J., Rabin, D., & Lynch, D. 1990, ApJ, 353, 712
Foukal, P., Little, R., & Mooney, J. 1989, ApJ, 336, L33
Frazier, E. N. 1971, Sol. Phys., 21, 42
Gingerich, O., Noyes, R. W., Kalkofen, W., & Cuny, Y. 1971, Sol. Phys., 18, 347
Hasan, S. S., Kalkofen, W., & Steiner, O. 1999, in Solar Polarization, ed. K. Nagendra, & J. Stenflo, Vol. 243 (Kluwer Academic Publishers), 409
Hirayama, T. 1978, PASJ, 30, 337
Hirayama, T. 1992, Sol. Phys., 137, 33
Keil, S. L., & Muller, R. 1983, Sol. Phys., 87, 243
Keller, C. U., Schüssler, M., Vögler, A., & Zakharov, V. 2004, ApJ, 607, L59
Keller, C. U., Steiner, O., Stenflo, J. O., & Solanki, S. K. 1990, A&A, 233, 583
Kneer, F., & Trujillo-Bueno, J. 1987, A&A, 183, 91
Knölker, M., Schüssler, M., & Weisshaar, E. 1988, A&A, 194, 257
Lawrence, J. K. 1988, Sol. Phys., 116, 17
Lites, B. W., Scharmer, G. B., Berger, T. E., & Title, A. M. 2004, Sol. Phys., 221, 65
Mehltretter, J. P. 1974, Sol. Phys., 38, 43
Minasyants, T. M. 1986, Solnechnye Dann. Bull. Akad. Nauk SSSR, 3, 88
Moran, T., Foukal, P., & Rabin, D. 1992, Sol. Phys., 142, 35
Muller, R. 1977, Sol. Phys., 52, 249
Nishikawa, J., & Hirayama, T. 1990, Sol. Phys., 127, 211
Ortiz, A., Solanki, S. K., Domingo, V., Fligge, M., & Sanahuja, B. 2002, A&A, 388, 1036
Scharmer, G. B., Bjelksjö, K., Korhonen, T., Lindberg, B., & Petterson, B. 2003, in Innovative Telescopes and Instrumentation for Solar Astrophysics, ed. S. Keil, & S. Avakyan, SPIE Proc., 4853-47 (Washington: Bellingham), 341
Schroeter, J. D. 1789, Beobachtungen über die Sonnenfackeln und Sonnenflecken (Erfurt: Georg Adam Keyser)
Schüssler, M. 1986, in Small Scale Magnetic Flux Concentrations in the Solar Photosphere, ed. W. Deinzer, M. Knölker, & H. H. Voigt (Göttingen: Vandenhoeck & Ruprecht), 103
Secchi, P. A. 1872, Die Sonne, ed. H. Schellen (Braunschweig: Druck und Verlag von George Westermann)
Solanki, S. K. 1986, A&A, 168, 311
Spruit, H. C. 1974, Sol. Phys., 34, 277
Spruit, H. C. 1976, Sol. Phys., 50, 269
Spruit, H. C. 1977, Sol. Phys., 55, 3
Steiner, O., Grossmann-Doerth, U., Knölker, M., & Schüssler, M. 1998, ApJ, 495, 468
Steiner, O., & Stenflo, J. O. 1990, in IAU Symp., 138, 181
Sütterlin, P., Wiehr, E., & Stellmacher, G. 1999, Sol. Phys., 189, 57
Ten Bruggencate, P. 1940, ZAp, 19, 59
Unsöld, A. 1938, Physik der Sternamosphären, mit besonderer Berücksichtigung der Sonne (Berlin: Verlag von Julius Springer)
Vogler, F., Brandt, P., Otruba, W., & Hanselmeier, A. 2004, in Solar Magnetic Phenomena, ed. A. Hanselmeier, A. Veronig, & M. Messerotti, Proc. Kanzelhöhe summer school 2003 (Kluwer), in press
Waldmeier, M. 1949, ZAp, 26, 147
Wang, H., Spirock, T., Goode, P. R., et al. 1998, ApJ, 495, 957
Wang, H., & Zirin, H. 1987, Sol. Phys., 110, 281
Yudina, I. V. 1976, Solnechnye Dann. Bull. Akad. Nauk SSSR, 2, 88